BWROG-TP-12-019
Revision 0
October 2012

Task 1 - CFD Report and Combined NPSHr Uncertainty for Monticello RHR CVDS Pump

Author:	Ankur Kalra (Sulzer Pump)
Project Manager:	Kenneth Welch (GEH)
Committee Chairman:	John Freeman (Exelon)

INFORMATION NOTICE

BWROG Utility Members	
CENG – Nine Mile Point	Chubu Electric Power Company
DTE – Fermi	Chugoku Electric Power Company
Energy Northwest – Columbia	Comisión Federal de Electricidad
Entergy – FitzPatrick	Hokuriku Electric Power Company
Entergy – Pilgrim	Iberdrola Generacion, S.A.
Entergy – River Bend/Grand Gulf	Japan Atomic Power Company
Entergy – Vermont Yankee	J-Power (Electric Power Development Co.)
Exelon (Clinton)	Kernkraftwerk Leibstadt
Exelon (D/QC/L)	South Texas Project
Exelon (Oyster Creek)	Taiwan Power Company
Exelon (PB/Limerick)	Tohoku Electric Power Company
FirstEnergy – Perry	Tokyo Electric Power Company
NPPD – Cooper	
NextEra – Duane Arnold	
PPL – Susquehanna	
PSEG – Hope Creek	
Progress Energy – Brunswick	
SNC – Hatch	
TVA – Browns Ferry	
Xcel – Monticello	

Executive Summary

This BWROG Technical Product provides a summary of the results of Computational Fluid Dynamics (CFD) studies to model uncertainties in $NPSH_R$ for the CVDS model pump used in the Monticello RHR system, an analysis of the limitations of state-of-the-art CFD codes in predicting pump $NPSH_R$, alternative methods for evaluating the individual $NPSH_R$ uncertainty terms, and a method for combining the individual uncertainty terms to determine an overall pump $NPSH_R$ uncertainty.

Implementation Recommendations

This product is intended for use to address (in part) issues raised in the NRC Guidance Document for the Use of Containment Accident Pressure in Reactor Safety Analysis (ADAMS Accession No. ML102110167). Implementation will be part of the BWROG guidelines on the use of Containment Accident Pressure credit for ECCS pump NPSH analyses.

Benefits to Site

This product provides a technical response to the NRC questions about how utilities account for the uncertainties in pump $NPSH_R$ when evaluating ECCS pump performance in accident conditions.

SULZER

QUALITY LEVEL

☐ Direct
☐ Indirect

SULZER PUMPS (US) INC. DOCUMENT

DOC. NO: E12.5.1959

ORDER NO: 100072780

TITLE: Task 1 - CFD Report and Combined NPSHr Uncertainty for Monticello RHR CVDS Pump

Sulzer Pumps (US) Inc.
Monticello – RHR Pumps

ASME CODE SECTION

CLASS NO.

CODE EDITION (YEAR)

SEASON YEAR

CUSTOMER GE-HITACHI Nuclear Energy Americas LLC

PROJECT Monticello Nuclear Power Station, Monticello, MN

CUSTOMER P.O. NO. 437054820

CONTRACT NUMBER

SPECIFICATION NO.

ITEM / TAG NUMBER

CUSTOMER APPROVAL NUMBER:

SPACE FOR CUSTOMER APPROVAL STAMP
(when applicable/available)

CUSTOMER APPROVAL REQUIREMENT

☐ Yes ☐ No ☑ Information Only

CERTIFIED AS A VALID SULZER PUMPS (US) INC. DOCUMENT

☐ For Outside Vendor

☒ For Manufacture at Sulzer Pumps (US) Inc.

☐ Risk Release Inspection Report # ______

☐ Other (specify) ______

APPROVALS (SIGNATURE)		Date
Engineering		09/28/12

CERTIFICATION (when applicable)

This Document is certified to be in compliance with THE APPLICABLE PURCHASE ORDER, SPECIFICATIONS, PROCEDURES, AND ADDITIONAL REQUIREMENTS LISTED IN THE APPENDICES.

______
Professional Engineer

______ ______
State Registration No.

Date ______

Originating Dept: Advance Engineering

By: Daniel Baun & Ankur Kalra

Title: Manager & Hydraulic Design Engineer

Date: 06/18/2012

APPLICABLE S.O. NUMBERS:
0

DOCUMENT IDENTIFICATION	Rev.
E12.5.1959	0

TABLE OF CONTENTS

1.0 CFD ANALYSIS

A computational fluid dynamics (CFD) analysis of the Monticello 12x14x14.5 CVDS pump was undertaken with the objective of quantifying the effect of various pump and system parameters on the pump's required Net Positive Suction Head (NPSHr) characteristic. In part, the analysis was intended to establish the efficacy of CFD in quantifying the individual influence as well as the combined influences of the following variables on the pump NPSHr: 1) plant piping geometry 2) fluid temperature 3) dissolved gas and 4) wear ring clearance.

The modeled 12x14x14.5 CVDS pump is used at Monticello as a Residual Heat Removal (RHR) system pump and is a vertically arranged overhung single stage double suction centrifugal pump configured with a double volute and in-line suction and discharge nozzles. The pump uses a four vane non-staggered impeller design with an inlet vane tip diameter of [[ ]]. The overhung impeller is cantilevered off a short stub shaft that is supported in a product lubricated bearing before being rigidly coupled to the shaft of the drive motor. The full diameter pump specific speed ($Ns = RPM*Q^{0.5}/H^{0.75}$) is [[ ]] (based on total pump flow) and the suction specific speed ($Nss = RPM*\{0.5*Q\}^{0.5}/NPSHr^{0.75}$) is [[ ]] (based on flow per impeller eye). Figures 1, 2, 3, and 4 show the CFD geometric model and the mesh characteristics are provided in Tables 1 and 2. The full diameter pump characteristic curves are shown in Figure 5.

1.1 CFD Model and Simulation Set-Up

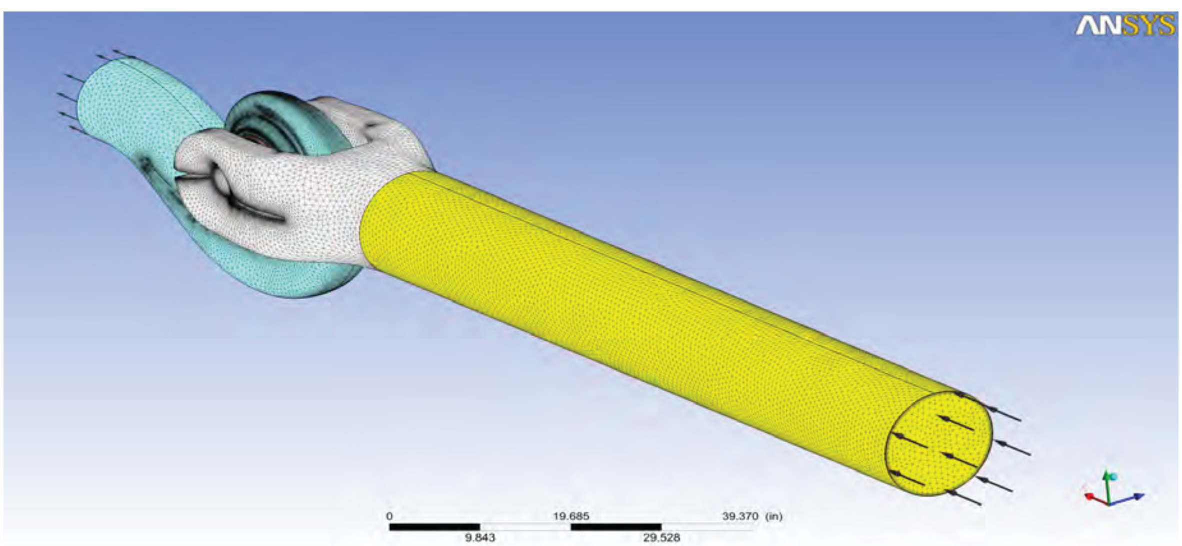

Figure 1: Monticello CVDS CFD Model - Isometric View

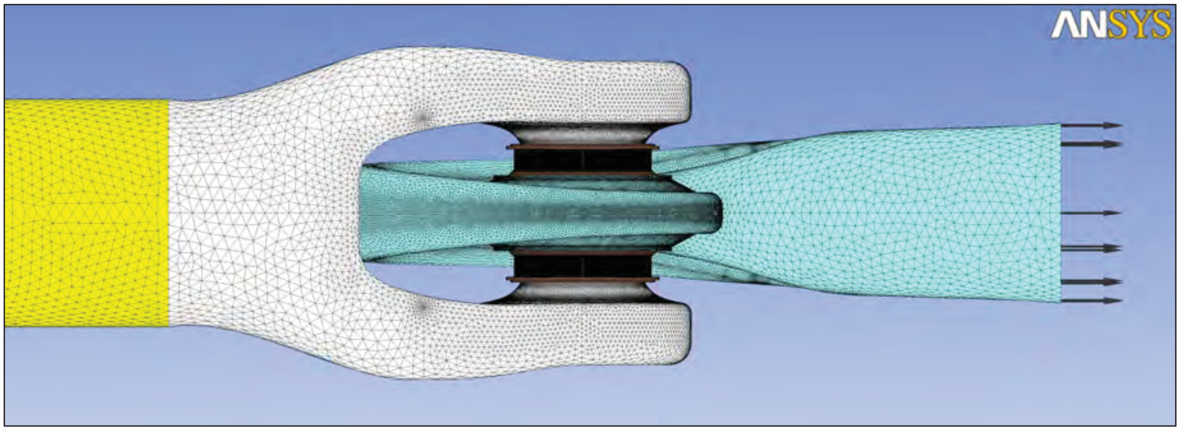

Figure 2: Monticello CVDS CFD Model - Side View

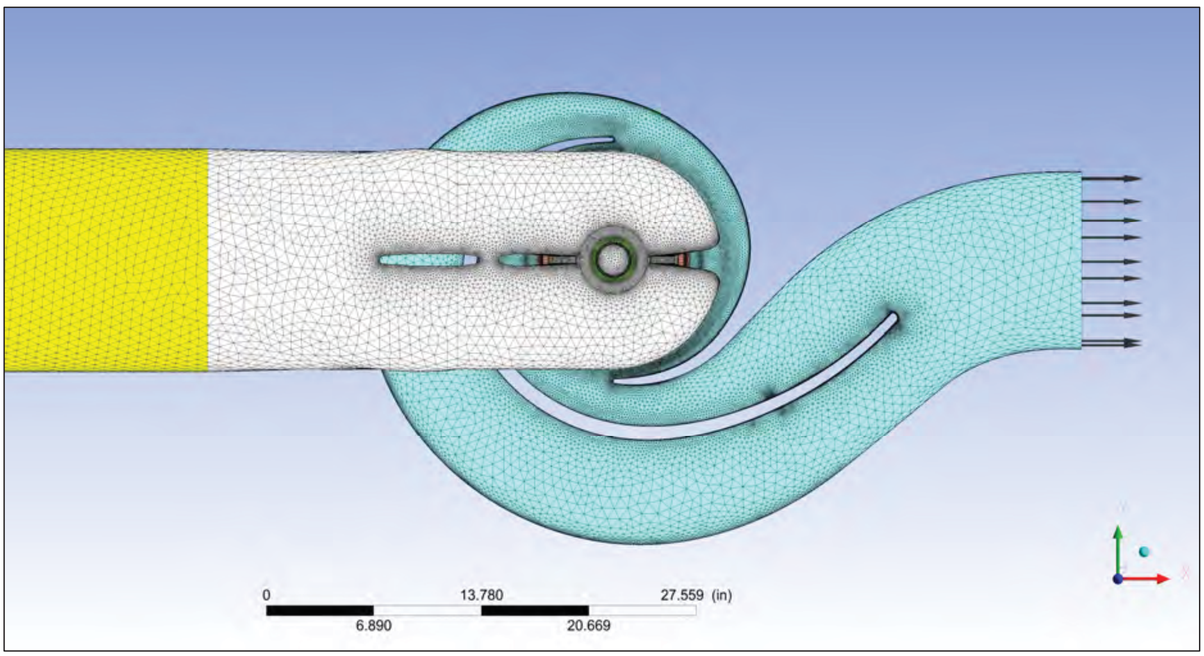

Figure 3: Monticello CVDS CFD Model - Plan View

[[

]]

Figure 4: Monticello CVDS CFD Model - Impeller Eye Ring Detail

Item	Setting
Code Type	[[
Turbulence	
Advection Scheme	
Cavitation	
Inlet B.C.	
Outlet B.C.	
Simulation Type	
MFR Setting	]]

Table 1: Monticello CVDS CFD Model Grid/Mesh Statistics

Domain	Node Count	Element Count
Pipe	[[	
Suction		
Impeller		
Seals		
Volute		]]

Table 2: Monticello CVDS CFD Model Grid/Mesh Statistics

[[ ]] The CFD code employed on the project was ANSYS CFX, a well-documented and validated commercial RANS (Reynolds Averaged Navier Stokes) based finite volume general purpose CFD solver. The key CFD solver set-up and configuration metrics are given in Table 1. The CFD mesh statistics are provided in Table 2. A hybrid grid constructed from approximately [[ ]] elements was used in the full CFD model.

1.2 Discussion of CFD Results

A baseline set of CFD simulations was run at flow rates (Q) of [[ ]] gallons per minute (gpm) to compare with the tested pump curve. These flows correspond to normalized pump flows (Q*) of [[ ]], respectively. The normalized flow (Q*) is defined as the flow rate (Q) divided by the best efficiency flow (Q_{BEP}), $Q^* = Q/Q_{BEP}$. The baseline CFD model included the complete pump geometry with a straight inlet pipe as illustrated in Figure 1 and was run as a steady-state simulation with Frozen Rotor grid interfaces applied at both the impeller inlet and exit.

Head and efficiency CFD results showed excellent agreement with the manufacturer's test bed measured performance as shown in Figure 5. However, the NPSHr results from the CFD simulations compared poorly with the measured 3% NPSHr values for the pump.

[[

]]

Figure 5: CFD Overlay with Test Data (Normalized to Full Diameter)

The poor NPSHr comparison was attributed to limitations in the steady-state model in simulating the intrinsically unsteady nature of the flow field in this CVDS pump. This resulted in poor model convergence. Two primary contributors to unsteady flow were identified:

a. Geometric asymmetry between the two halves of the double suction impeller resulting in flow asymmetry between the two impeller inlets (eyes). On one side of the impeller, the shaft protrudes through the impeller eye, whereas it is absent on the opposite side of the impeller.
b. Strong interaction between the impeller exit and the volute lips associated with the exit Frozen Rotor grid interface and the relative clocking position of the impeller vanes relative to the volute lips. These effects are visible in Figure 6 and Figure 7. Figure 6 shows velocity streamlines on a planar slice through the middle of the pump (plane of symmetry). The color levels indicate velocity magnitude. Visible in this figure are regions of flow separation and recirculation within the volute passages. Figure 7 shows the associated variation in the pump discharge pressure at a particular element in the mesh as the CFD solution bounces about its converged solution. The total variation in the pump discharge pressure at this monitor point is very high, approximately [[ ]], and is indicative of a poorly converged CFD result.

[[

]]

Figure 6: Flow Streamlines at BEP

[[

]]

Figure 7: Total Pressure at Volute Outlet

In many unsteady applications, a steady-state CFD modeling approach will provide satisfactory results. A steady-state CFD solution to a physically unsteady problem (flow through a centrifugal pump) attempts to approximate a flow field solution without changing the relative orientation of the moving segment of the domain (impeller) with respect to stationary segments of the domain (inlet casing and volute) during the solution process. To do this, the steady-state approach must impose nonphysical approximations to the solution process that affect the simulated results. There are two standard techniques used to handle the transfer of flow variables across the grid interfaces (between rotating and stationary segments of computational domain) in a steady-state approximation of a transient problem: the Frozen Rotor interface (which was used in the baseline case) and the Stage interface.

a. The Frozen Rotor interface approximation solves the pump flow field as if the effects of the relative position (angular clocking) between the rotating domain (impeller) and the stationary domain (inlet and volute) are fixed in the discrete orientation that the CFD model was constructed in. This means the relative angular position of any particular impeller vane with respect to a volute lip(s) will not change during the solution process. However, the impeller to volute discrete angular clocking position will affect the resultant volute pressure field and correspondingly affect the pressure and flow fields in each impeller vane passage. In the case of a flow asymmetry arriving at a Frozen Rotor interface (e.g., piping induced flow asymmetry at the impeller inlet) the relative angular orientation between the flow asymmetry and a particular impeller vane will not change as the flow asymmetry is transferred across the interface.

b. The Stage interface approximation circumferentially averages the flow field variables as the flow transfers from one side of the interface to the other. The net result is that the influence of a geometric asymmetry (e.g., volute lip) will be averaged out of the flow field. In effect, the impeller sees the volute as a circumferentially symmetric device. Similarly, in the case of a flow asymmetry arriving at a Stage interface (e.g., piping induced flow asymmetry at impeller inlet) the flow asymmetry is circumferentially averaged (washed out) as it crosses the Stage interface into the impeller eye.

These grid interface connections are employed to approximate the real world transient physical phenomena with a quasi steady-state process so that a CFD problem can be solved in a reasonable length of time using available computer hardware resources.

An alternative to the steady-state approximations discussed above is to run a time transient CFD simulation. In a transient CFD simulation of a centrifugal pump, the angular orientation of the impeller relative to the stationary portion of the computational domain is indexed in discrete finite clocking positions. At each clocked position, a complete flow field solution is obtained. To reach convergence it is often necessary to simulate several complete impeller rotations. Thus, a single transient simulation requires from 25 to 50 times the computational effort as the corresponding steady-state approximation of the same problem depending on the angular resolution of the impeller clocking used. Time transient cases are very computer resource intensive and a single run may take several days to reach convergence.

A time transient simulation was run to test the efficacy of a time transient CFD analysis to determine the NPSHr of the Monticello CVDS pump and to determine if the poor comparison in the NPSHr simulation obtained from the steady-state simulation using the Frozen Rotor grid interfaces was indeed a consequence of flow unsteadiness coupled with the modeling approximations inherent in a steady-state modeling approach. Due to the high computational resources required for a time transient simulation, only one flow case [[ ]] was executed. Figure 8 presents the comparison of the simulated transient results and the baseline steady-state model case at [[ ]]. From Figure 8, it is seen that the 3% head breakdown for the transient simulation is approximately [[ ]], which is a considerable improvement compared to the [[ ]] value derived in the steady-state case, yet still remains relatively higher than the tested value of [[ ]]. This exercise suggests that time transient CFD analysis would be a more appropriate simulation method for the Monticello CVDS pump. However, the precision necessary to do further NPSHr analysis required by the project was still lacking with respect to the test results, and the resources and computing effort required to conduct a full transient CFD analysis of the scope required by this project was prohibitively high. In view of this, several variants of steady-state models were investigated as discussed below to determine if an alternate approach was feasible.

[[

]]

Figure 8: Transient Simulation at [[ ]] Cavitation Breakdown Overlay with Baseline – Full Model Steady-State Simulation Result

1.3 CFD Modeling Variants

In an attempt to reach a workable compromise between solution fidelity and analysis time/cost, several variations to both the steady-state set-up used in the CFD analysis as well as to the 3D pump geometry used in the CFD model were investigated. Table 3 lists the CFD cases and variations that were investigated. In the following sections of the report each CFD variant and its respective result are presented in detail.

CFD Model Variant No.	Solver & Model Description	Grid Interface Settings
Baseline	CFX - Full Model with Volute	Frozen Rotor Interface at both Impeller Inlet and Exit
1	CFX - Impose Plane of Symmetry to Full Pump Geometry.	Frozen Rotor Interface at both Impeller Inlet and Exit
2	CFX - Plane of Symmetry Model with Volute replaced by Pinched Vaneless Diffuser.	Stage Interface at Impeller Exit. Frozen Rotor Interface at Impeller Inlet.
3	CFX - Plane of Symmetry Model with Volute replaced by Pinched Vaneless Diffuser.	Stage Interface at both Impeller Inlet and Exit
4	STAR CCM+ (Full Model with Volute)	Frozen Rotor Interface at both Impeller Inlet and Exit w/ Unsteady Cavitation Model

Table 3: CFD Modeling Variants

1. CFD Model Variant No. 1

The unsteadiness in the steady-state CFD solution and the resultant poor NPSHr comparison was possibly due to variations in the flow between the two sides of the impeller arising from variations in the physical geometry between the inlets on the two sides of the impeller. As discussed previously, the Monticello RHR CVDS pump has a single stage double suction impeller cantilevered off the drive shaft. In this design, the shaft protrudes through the eye on one side of the impeller, but is absent the opposite side. Except for this variation, the Monticello RHR CVDS pump geometry is symmetrical about a plane as illustrated in Figure 9. By imposing this plane of symmetry in the CFD model, the potential for asymmetric flow between the two sides of the impeller was eliminated. Consequently, the suspected contribution of asymmetric flow to the unsteadiness in the CFD solution was also eliminated. The plane of symmetry simplification also reduced the overall size of the CFD model by a factor of ½.

Using the plane of symmetry simplification, a CFD simulation was run at [[ ]]. The CFD results are shown in Figure 10 and no appreciable improvement in the predicted NPSHr is seen. Convergence problems persisted and it was concluded that the plane of symmetry simplification did not address unsteadiness arising from the impeller exit flow interaction with the volute lips or the recirculating flow in the volute.

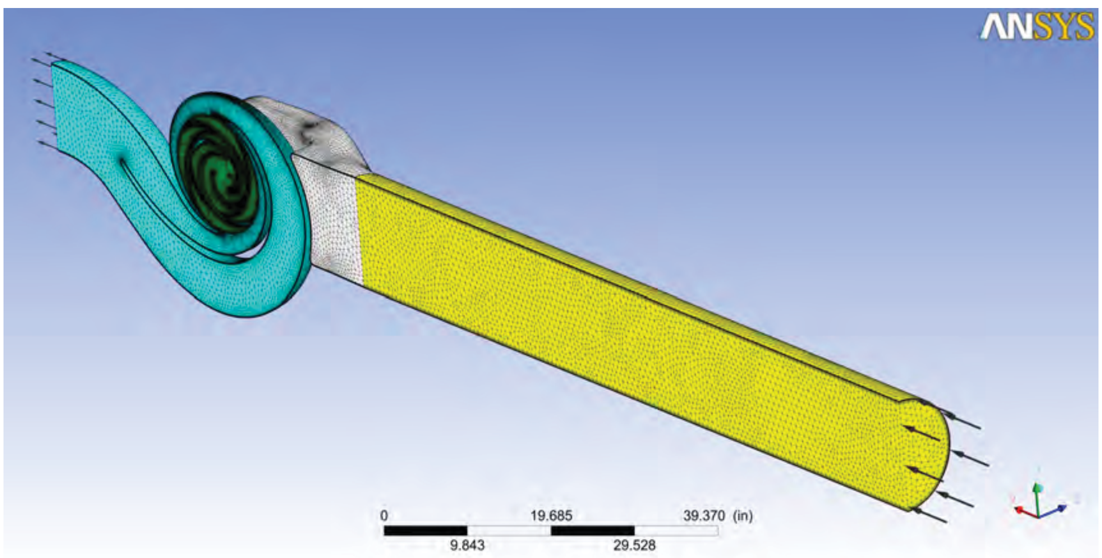

Figure 9: Plane of Symmetry Model with Volute

[[

]]

Figure 10: [[ ]] **Cavitation Breakdown Overlay between Full Pump Model and Plane of Symmetry Model (Steady-State Simulation with Frozen Rotor Interfaces at both Inlet and Exit)**

2. CFD Model Variant No. 2

As discussed in Section 1.2, the Frozen Rotor grid interface fixes the relative angular clocking between the impeller and the volute (or inlet casing) in one discrete relative angular position. The relative angular position of any particular impeller vane with respect to a volute lip will affect the resultant volute pressure field and consequently affect the pressure and flow fields in each impeller vane passage. The simulated impeller passage flow and pressure fields will have a corresponding effect on the degree of cavitation development on each impeller vane as the available Net Positive Suction Head (NPSHa) is reduced. This effect is illustrated in Figure 11 and Figure 12, which show the cavitation development on the impeller vane tips at two NPSHa levels from the plane of symmetry model simulation case. Figure 11 shows that the cavitation development on all four impeller vane tips is relatively uniform at [[ ]] NPSHa. This contrasts with the cavitation development in Figure 12 at [[ ]] NPSHa where the developed cavitation (bubble length) is no longer uniform. The circular symmetry in the blade-to-blade cavitation development shown in Figure 11 is replaced by the situation in Figure 12 where 2 opposing vanes show extensive cavitation while the remaining 2 opposed vanes have relatively less cavitation. A 3% head breakdown condition due to cavitation generally occurs when the developed cavitation "bubble" extends from the blade leading edge to the inlet throat location which occurs at the overlap of the adjacent vane. The cavitation illustrated in Figure 12 would imply complete head breakdown on two vanes (cavitation bubble fills entire vane passage) and virtually no head breakdown on the other two vanes. This asymmetric cavitation development may be related to the relative angular clocking position between the two volute lips (double volute) and the 4 impeller vanes. Small temporal and spatial variations in the blade-to-blade cavitation development can be expected as a result of the normal vane pass pressure pulsations created each time an impeller vane passes by a volute lip. However, the degree of variance in the blade-to-blade cavitation development illustrated in Figure 12 is nonphysical and is likely a primary reason for the poor NPSHr prediction using the plane of symmetry CFD model (steady-state simulation with Frozen Rotor grid interfaces). Additionally, the same level of flow unsteadiness illustrated in Figure 6 still existed in the CFD solution.

[[

]]

Figure 11: Cavitation Development at Impeller Inlet – NPSHa = [[ ]]

[[

]]

Figure 12: Cavitation Development at Impeller Inlet – NPSHa = [[ ]]

In an attempt to address both the persistent solution unsteadiness and the suspected cause of the asymmetric blade inlet cavitation development (asymmetric back pressuring of impeller due to angular position of individual impeller passages relative to volute lips combined with Frozen Rotor interface when using steady-state approximation), the pump volute was removed from the computational domain and replaced with a pinched radial vaneless diffuser as shown in Figure 13. A pinched radial vaneless diffuser is turbomachinery nomenclature for a concentric empty space arranged around the impeller outer diameter with a converging cross-sectional profile as the radius increases. The converging cross-sectional profile is used to control the flow area and, thereby, the diffusion rate as the flow moves radially outward from the impeller exit. By limiting the diffusion rate, the flow is prevented from stalling, which can cause additional CFD convergence issues. The intended effects of this change are two fold: 1) the unsteady recirculation regions in the volute will be removed, and 2) to affect the asymmetric blade inlet cavitation development by removing the back pressuring effect caused by the discrete angular clocking between the volute lips relative to the impeller vanes (a consequence of the Frozen Rotor grid interface at the impeller exit). With the pump volute replaced by a symmetric radial vaneless diffuser, the grid interface between the impeller and the volute was changed to a Stage interface.

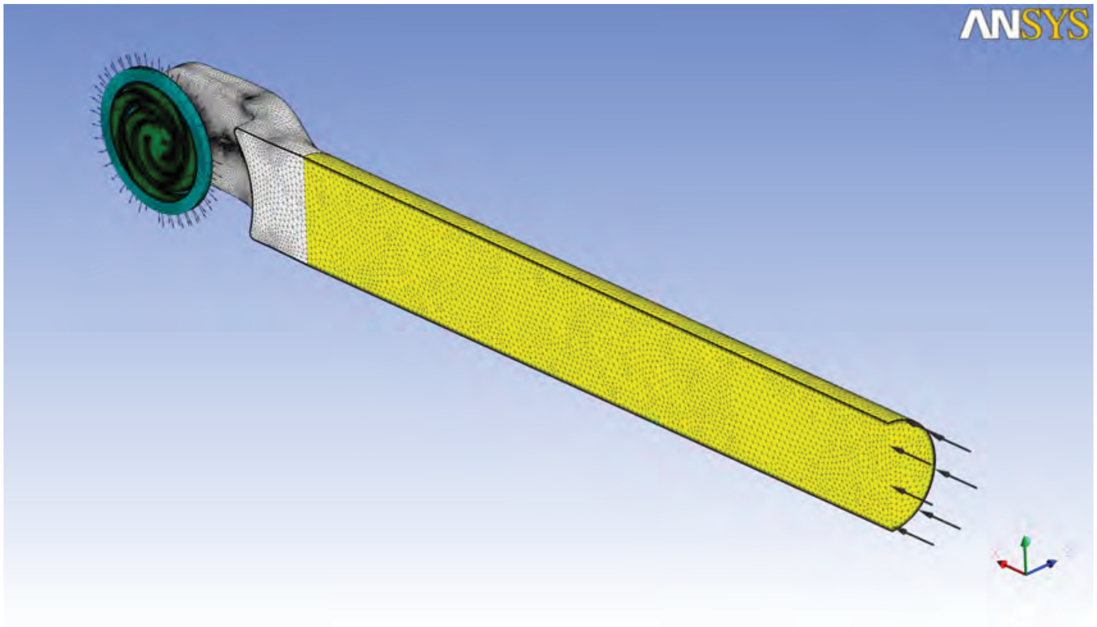

Figure 13: Plane of Symmetry Model with Pinched Vaneless Diffuser

Using this new set-up, plane of symmetry with pinched vaneless diffuser combined with Stage interface setting at impeller exit and Frozen Rotor interface setting at impeller inlet, a simulation was run at [[ ]]. The results from this simulation are compared with the baseline simulation and the plane of symmetry simulation in Figure 14. No appreciable change in the NPSHr prediction was achieved with this new set-up compared to the previous simulations. However, the absolute value of the pump discharge head was reduced by approximately [[ ]] with the pinched diffuser compared to the volute. There are two possible explanations for this result. First, despite the presence of large recirculation zones within the volute channels for the previous simulation cases (Figure 6), the overall effect of this recirculation on the losses may be relatively minor. Second, when using the volute and the Frozen Rotor grid interface, the simulated pump discharge head will depend on the relative angular clocking position between the impeller and the volute lips. It is possible that the impeller to volute clocking position used for the volute model simulations produced a head that was greater than the head that would have been obtained if a calculated average was used. In this case, the calculated average would have been based on the results of several simulations where the discrete angular clocking between the impeller and the volute was systematically indexed to represent one impeller blade passage transiting a volute lip (a 90 degree segment in this case). The use of a pinched vaneless diffuser and a Stage grid interface removes the dependence of the simulated pump head on the relative angular clocking of the impeller as described in the introductory discussion to this section.

[[

]]

Figure 14: [[ ]] **Cavitation Breakdown Overlay between Full Pump Model, Plane of Symmetry Model using Volute, and Plane of Symmetry Model using Pinched Vaneless Diffuser with Frozen Rotor Interface at Impeller Inlet**

3. CFD Model Variant No. 3

Based on the results from the pinched radial vaneless diffuser case using the Frozen Rotor interface at the Impeller inlet and Stage interface at the impeller exit, the asymmetry observed on the blade cavitation development in Figure 11 and Figure 12 can not be entirely attributed to the effect of the volute casing when using the Frozen Rotor grid interface at the impeller exit. Therefore, the impeller inlet flow fields from the pinched vaneless diffuser simulation case were further examined. Figure 15 shows that an asymmetric inlet velocity profile exists at the impeller eye. Initially, it was hypothesized that this asymmetric inlet velocity profile was a result of volute back pressuring (Frozen Rotor grid interface between impeller and volute). However, since this asymmetric inlet velocity profile persisted after the volute was replaced with the pinched vaneless diffuser and the Stage interface at the impeller exit, it was concluded that the inlet asymmetry must arise from the inlet casing coupled with the Frozen Rotor interface at the impeller inlet.

[[

]]

Figure 15: Inlet Axial Flow and Total Pressure Distribution at Impeller Eye (Plane of Symmetry with Pinched Vaneless Diffuser with Stage Interface at Impeller Exit and Frozen Rotor Interface at Impeller Inlet)

Hence, the asymmetric inlet flow field shown in Figure 15 must be a result of the flow splitters used in the inlet casing design coupled with the use of the Frozen Rotor grid interface at the impeller inlet since the influence of volute lips and the Frozen Rotor interface at impeller exit have been removed. The inlet casing flow splitters are visible as dark shadows protruding into Figure 15 at the 12:00 O'clock and 6:00 O'clock positions. Note that there is a large variation in the axial velocity profile (left side of Figure 15) whereas the total pressure profile is nearly uniform across the whole impeller inlet (right side of Figure 15). Flow asymmetry at the impeller inlet will lead to non-uniform incidence and velocity distributions at the impeller vane leading edges, which, in turn, will result in non-uniform cavitation development on the inlet portion of vanes as NPSHa is reduced. In an attempt to remove the influence of the inlet casing flow splitters on the impeller inlet flow field and the subsequent asymmetric cavitation development, the Frozen Rotor grid interface at the impeller inlet was replaced with a Stage interface. A CFD simulation was run at [[ ]] and the results are displayed in Figure 16. As can be seen in this figure, the predicted NPSHr showed some improvement. The predicted NPSHr is approximately [[ ]] (extrapolated the simulated breakdown knee to 3% head breakdown). While this is an improvement over the previous simulations that used a Frozen Rotor interface at the pump inlet, it is still well short of the tested NPSHr value of [[ ]].

[[

]]

Figure 16: [[ ]] **Cavitation Breakdown Overlay between Full Pump Model, Plane of Symmetry Model using Volute, Plane of Symmetry Model using Pinched Vaneless Diffuser w/ Frozen Rotor Interface at Impeller Inlet and Plane of Symmetry Model using Pinched Vaneless Diffuser w/ Stage Interface at Impeller Inlet**

The blade cavitation development resulting from this CFD modeling variant, Stage interface at pump inlet, is shown in Figure 17. In comparing Figure 17 with Figure 11 and Figure 12, while it is apparent that the vanes experiencing the heaviest cavitation have shifted by 90 degrees, the general character of the cavitation development remained much the same.

[[

]]

Figure 17: Cavitation Development at Impeller Inlet (Pinched Vaneless Diffuser with Stage Grid Interface at Impeller Inlet)

An explanation for what has happened at the pump inlet when the Stage interface was imposed can be determined by examining the corresponding velocity and total pressure contours for this simulation, which are shown in Figure 18. The inlet casing flow splitters are again visible as dark shadows protruding into the figure at the 12:00 O'clock and 6:00 O'clock positions. It is clear from the top left contour plot in Figure 18 that some minor axial flow asymmetry is being induced by the inlet casing. However, this asymmetry is washed out by the Stage grid interface as is shown by the bottom left plot in the figure. The bottom right contour plot in Figure 18 clearly shows the influence of the suction casing flow splitters on the total pressure distribution on the impeller side of the inlet Stage interface. This total pressure contour contrasts with the corresponding total pressure contour from Figure 15 (CFD Model Variant No. 3, the pinched vaneless diffuser case with the Frozen Rotor grid interface at the pump inlet). The static pressure distribution at the impeller eye (impeller side of interface) will be similar to the total pressure distribution due to the near uniform axial velocity distribution (bottom left plot in Figure 18). The net result is the asymmetric cavitation bubble lengths as illustrated in Figure 17.

[[

]]

Figure 18: Axial Velocity and Pressure Contours Across Stage Grid Interface at Impeller Inlet (negative number denotes outflow from suction casing)

4. CFD Model Variant No. 4

In addition to the above CFD variant cases using ANSYS CFX, an alternative CFD code, STAR CCM+, was tested. The STAR CCM+ CFD code was configured with an unsteady cavitation model while the balance of the simulation was run as steady-state simulation using Frozen Rotor grid interface settings. Initially, it was believed that the STAR CCM+ CFD code, using this enhanced cavitation model, could solve the Monticello CVDS pump problem in a fraction of the time that it took the fully transient ANSYS CFX simulation to run while providing similar NPSHr simulation fidelity. However, after a complete cavitation knee head breakdown curve at [[ ]] was generated using STAR CCM+ (see Figure 19), a reduction in computational time combined with good solution fidelity was not realized. The quasi-transient STAR CCM+ simulation predicted an NPSHr of [[ ]] from the ANSYS CFX transient simulation and [[ ]] from test data.

[[

]]

Figure 19: [[ ]] **Cavitation Breakdown Overlay between ANSYS CFX Baseline Model and STAR CCM+ with Transient Cavitation Model.**

5. Conclusions

None of the CFD modeling and geometry variations provided a sufficiently accurate NPSHr baseline for the Monticello CVDS pump. A full transient CFD approach showed some promise, however, there remained an offset of several feet of NPSHr compared to the test curve and the time needed for the transient case runs and availability of computational resources proved to be prohibitive. Without a validated CFD baseline, it was not possible to evaluate NPSHr uncertainty effects for plant inlet piping, fluid temperature, dissolved air, and wear ring clearance using CFD. At this point, a decision was made to abandon the CFD effort to model the Monticello CVDS pump. The balance of this report documents a qualitative analysis approach used to quantify the NPSHr uncertainty for the various parameters. Additionally, relevant information from a literature review of related pump tests, other CFD analyses, and applicable industry standards is presented.

2.0 Analysis of Parameter Effects on NPSHr

2.1 Effect of Inlet Geometry on NPSHr

Pump suction impeller design assumes that the flow into the impeller eye will be relatively smooth and free of any distortions or circumferential rotations. Disturbances in the flow pattern can lead to non-uniform, rotationally unsymmetrical velocity profiles at the impeller eye leading to unpredictable (generally adverse) flow incidence angles. Figure 20 illustrates the impact of flow incidence angle (i) on the suction performance of an impeller (usually designed such that i = 0 at, or slightly above, the BEP flow rate). As seen in Figure 20, NPSHr increases if the incidence angle is negative with respect to the blade and NPSHr decreases for a positive incidence angle.

The inlet geometry of a pump, which includes the suction casing, straight pipe runs, elbows, fittings, and valves, can impact the flow pattern of the fluid entering the impeller eye. To minimize the disturbances, Hydraulic Institute (HI) Standard 9.6.6 [8] lists good design practices for suction inlet piping. For instance, to reduce the impact of flow distortion caused by upstream elbows, and tees, HI recommends installing a straight suction pipe of length equal to five diameters upstream of the pump inlet nozzle. However, due to space constraints and other field requirements, suction inlet design recommendations can often not be fully met.

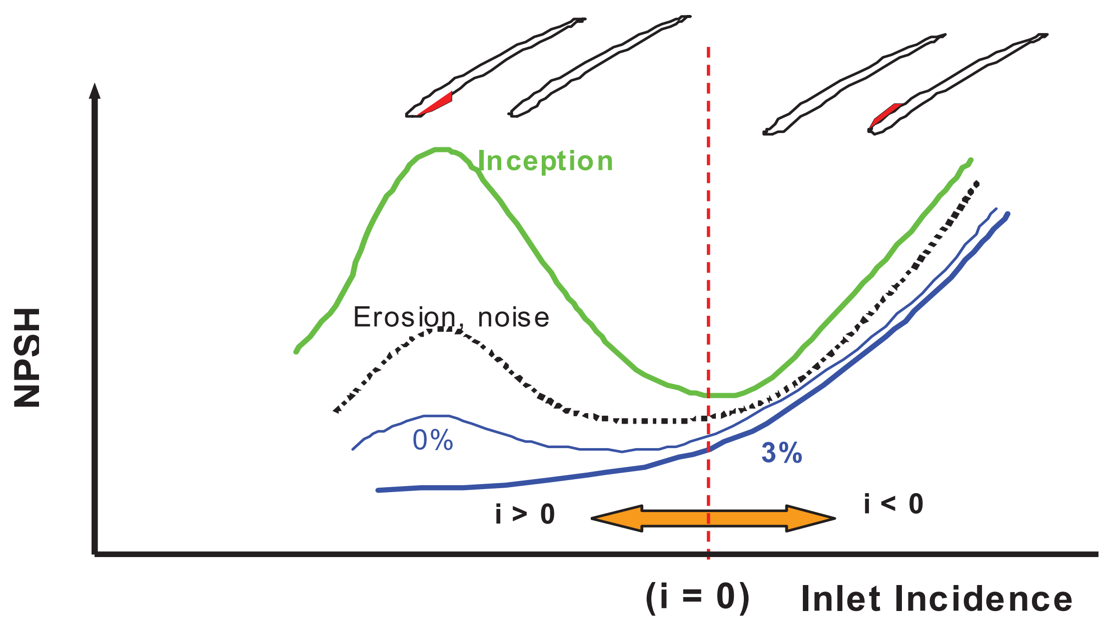

Figure 20: NPSH and Cavitation versus Inlet Incidence Angle

2.1.1 Literature Search Results

A German study by Roth [3] conducted at the Technical University of Darmstadt investigated the influence of an upstream suction piping elbow and a butterfly valve on the cavitation behavior of an axial inlet end suction centrifugal pump. Figure 21 shows the test set-up. A 90 degree pipe elbow and a butterfly valve with alternate valve disc orientations (vertical or horizontal) were positioned at different lengths upstream of the suction impeller. NPSHr tests were conducted for the below combinations. The straight pipe run (configuration GE) was used as the control set-up. The axial and circumferential components of the flow velocity at the inlet of the pump were measured using Laser Doppler Velocimetry (LDV).

Test #	Elbow	Valve Orientation	Distance of Elbow from Impeller
GE	No	No Valve	5 Pipe Diameters (5D)
0D-S	Yes	Vertical	0D
0D-K	Yes	Horizontal	0D
2D-S	Yes	Vertical	2D
2D-K	Yes	Horizontal	2D
5D-S	Yes	Vertical	5D
5D-K	Yes	Horizontal	5D

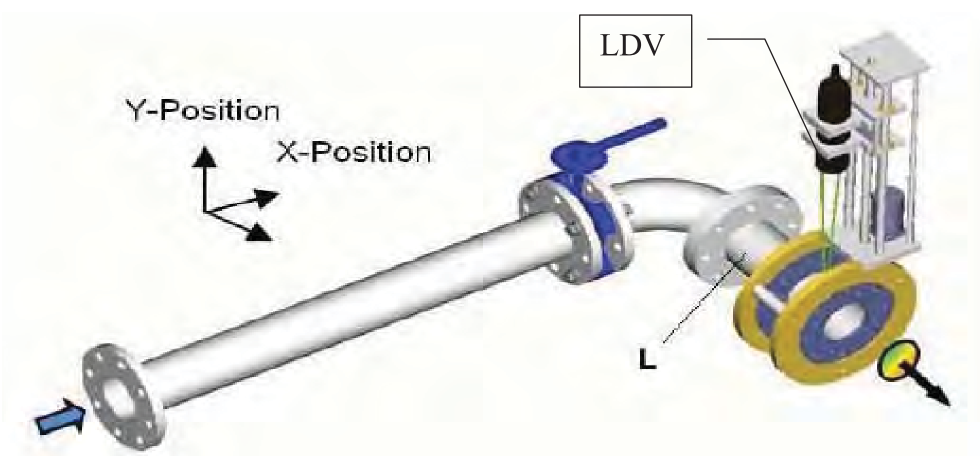

Figure 21: Test Set-up

The test results are plotted on Figure 22 as a function of normalized flow rate and show the influence of inlet piping geometry on the NPSHr of the pump. As seen in Figure 22, the straight pipe run case (GE) does not have the lowest NPSHr. Cases "0DS/2DS/5DS" (elbow with vertical valve orientation) provide better NPSHr performance than the control case. Piping set-up "0DK" (elbow and horizontal valve orientation at zero distance from the pump inlet) had the worst suction performance. At BEP, a maximum NPSHr difference of 0.7 meters (m) is observed between the straight pipe run (GE) and "0DK". Suction piping effects on NPSHr are greater at higher flow rates and a maximum impact of approximately 2 m is seen for case "0DK" at 120% of the BEP flow.

It can be hypothesized that the vertical orientation of the valve disc disrupts the pump inlet flow in a way that increases the incidence angle of the flow at the impeller inlet vanes and, thus, shifts the bubble growth to the suction surface of the blade reducing the effect of a given size bubble on NPSHr. Conversely, inlet piping combination "0DK" (elbow at pump suction and horizontal valve orientation) adversely impacts flow patterns and reduces the effective flow incidence angle in such a way as to shift the vapor bubbles to the pressure surface of the inlet vanes where a given sized bubble has a much greater relative effect on the NPSHr than it would have on the suction surface of the vane. At high flows the NPSHr for the DK cases increased by approximately 20% compared to the "GE" set-up. It is important to note that the impact on NPSHr observed in this study reflects a combined effect of flow disruptions caused by an elbow and a valve disc in the flow stream.

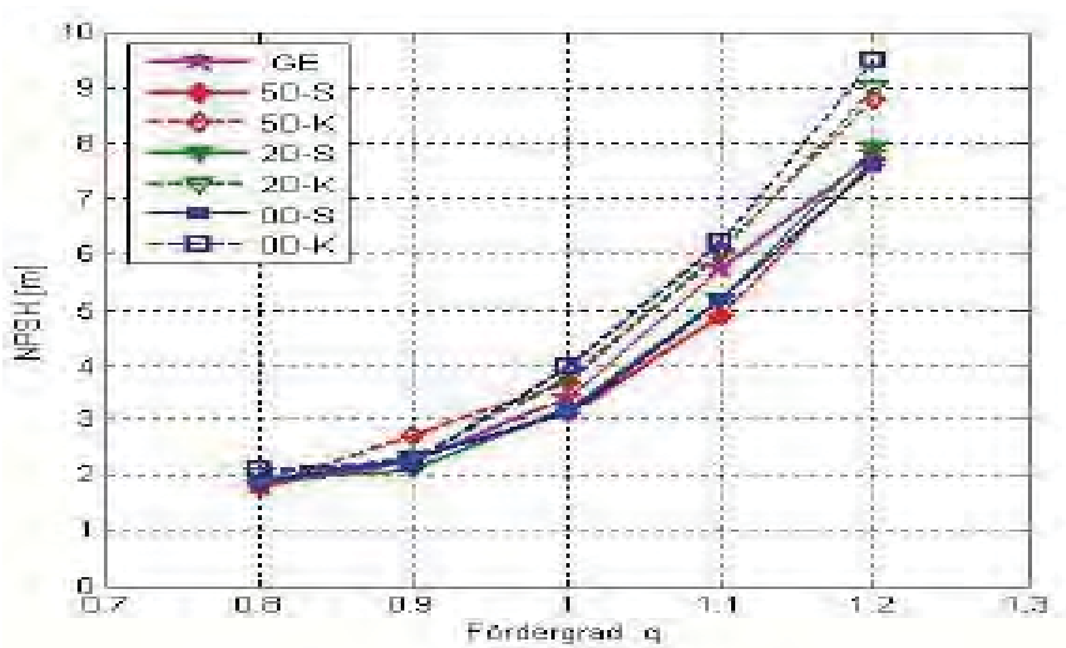

Figure 22: Impact of Inlet Geometry on NPSH3

Similar studies illustrating the influence of inlet piping on NPSHr have been published in several research papers. Schiavello [9] conducted visual inspections of the shape and size of cavitation bubbles on impeller blades to study the impact of swirling inlet flow. The study showed that the direction (clockwise versus counter-clockwise) of the swirling effect of inlet flow influenced cavitation performance. Bunjes and Op De Woerd [4] improved the inlet design of a double suction pump, which resulted in an NPSHr reduction of approximately 20%. Alan Budris and Mayleben [6] showed the impact of suction piping elbows on cavitation characteristics by recording the suction pressure pulsations. In their study, a straight pipe run was compared with a short radius elbow and then with two short radius elbows. Pump suction piping with two short radius elbows showed the worst performance with an increase of 54% in suction pulsations as compared to a straight run inlet.

2.1.2 Browns Ferry CFD Study on Suction Piping

A CFD study using ANSYS CFX software was conducted by Sulzer [5] to estimate the influence of inlet piping on the NPSHr of a Browns Ferry single suction CVIC RHR pump. The suction piping layout representing actual field configuration was modeled in 3-D as shown in Figure 23. CFD was used for predicting NPSHr for a straight inlet pipe run (length equal to seven pipe diameters) and then for the in-situ suction piping layout. The CFD analysis results provided in Figure 24 show an increase in NPSHr of [[ ]] for the field suction piping as compared to the straight run pipe.

[[

]]

Figure 23: Browns Ferry RHR Pump Suction Field Configuration and Control Set-up (straight run pipe)

[[

]]

Figure 24: CFD Analysis – Impact of Inlet Geometry on NPSHr of Browns Ferry CVIC Pump

2.1.3 Effects of Inlet Suction Design on NPSHr

Most public domain research work examining the effect of pump inlet piping configuration on NPSHr has focused on end suction pumps. End suction pumps do not have an inlet suction casing. The side inlet casings of double suction pumps, such as the Monticello RHR pump, are designed to smooth the flow by initially decelerating the flow in the casing and then accelerating the flow into the eye of the impeller. Further, a flow splitter (rib) is provided in an inlet casing to break any swirling flow patterns. Therefore, it is expected that the relative influence of inlet piping geometry variations on NPSHr for end suction pumps will be greater than the corresponding influence on pumps with suction casings.

Figure 25 shows a cross-sectional top view of a double suction inlet casing and illustrates the flow patterns at the impeller eye. This figure illustrates another important characteristic of side inlet casings. On one side of the casing a pre-rotation (rotation in the direction of the impeller rotation) is induced in the flow, which has the effect of reducing the blade incidence and shifting any bubbles toward the blade pressure surface. This contrasts with the situation on the opposite side of the impeller where a counter-rotation (rotation in the opposite direction as the impeller rotation) is induced on the flow. The counter-rotation has the effect of increasing the blade incidence and shifting the bubbles toward the blade suction surface. Therefore, each impeller eye side experiences different incidence and, thus, different NPSHr characteristics.

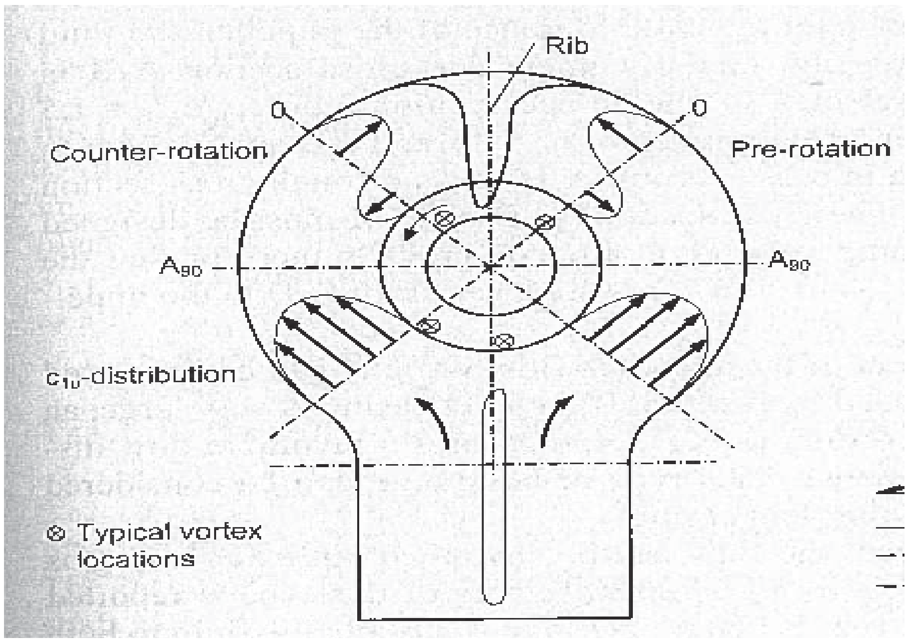

Figure 25: Suction Inlet Flow Pattern - Double Suction (Gulich)

2.1.4 Monticello Pump Suction Piping Configuration

The Monticello RHR pump field suction inlet piping configuration is shown in Figure 26. As seen in the figure, the distance between the tee and the 180 degree pipe bend is approximately nine pipe diameters (twice the HI recommendation). Therefore, any influence of the tee and/or any upstream flow distortion arriving at the tee should have minimal impact on the pump suction performance. The 180 degree pipe bend located at the inlet of the suction casing would be expected to cause flow distortions at the impeller eye. These distortions, also known as secondary flows, are created because of uneven pressure distributions in the bend as illustrated in Figure 27. It is important to note that the plane of the 180 degree bend and the secondary flow patterns are perpendicular to the plane of the flow splitters (the flow straightening devices shown in Figure 26) located in the suction inlet casing. Figure 28 and Figure 29 show how a vertical flow splitter is expected to interact with the secondary flow patterns and reduce the magnitude of distortions at the impeller eye. The effect of a flow splitter on NPSHr is similar to the effect of the butterfly valve orientation in the German study discussed above. Based on the results from the research on end suction pumps and the CFD analysis performed on the Browns Ferry RHR pump, which also has an inlet casing with a flow splitter, the impact of the in-situ inlet piping on the NPSHr of the Monticello CVDS Pump at rated pump flow of [[ ]] is expected to be in the range of [[ ]]. An averaged value [[ ]] is reasonable for use for NPSHr uncertainty considerations. A lower value is appropriate for more favorable suction piping configuration.

[[

]]

Figure 26: Monticello RHR Plant Inlet Piping Configuration

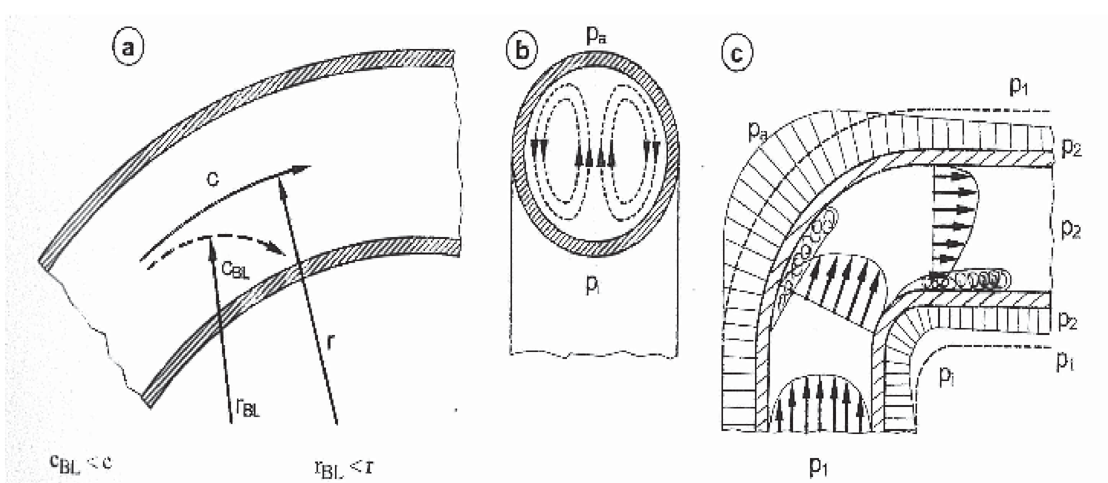

Figure 27: Secondary Flow Development in a Bend (Gulich)

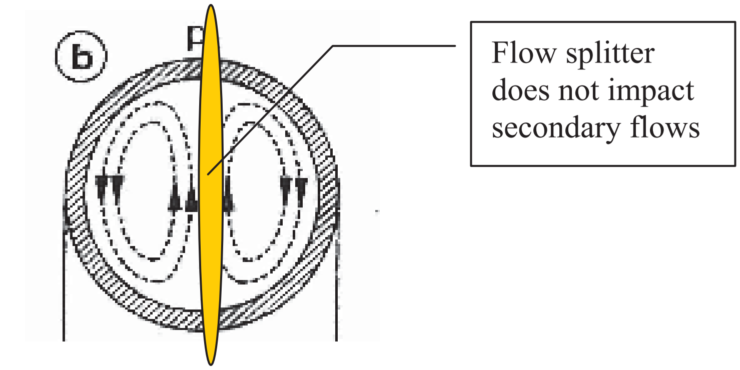

Figure 28: Flow Splitter Parallel to Plane of Elbow (Gulich)

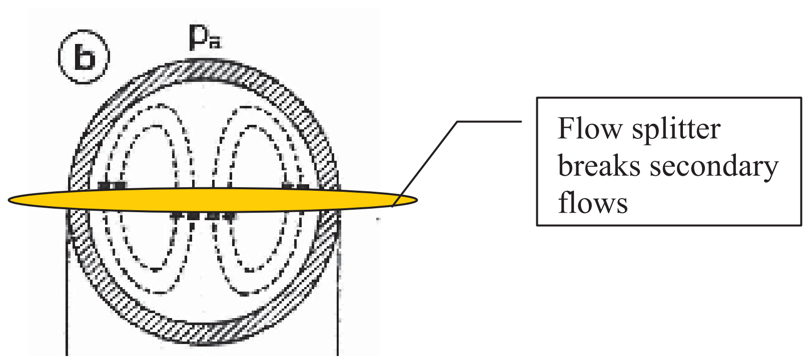

Figure 29: Flow Splitter Perpendicular to Plane of Elbow (Gulich)

2.2 Effect of Fluid Temperature on NPSHr

NPSHr reduces as the temperature of the pumped water increases. This behavior is explained by the phenomenon of thermal dynamic suppression head (TSH). As a fluid's temperature increases, the density of the vapor increases and, therefore, the amount of energy required to produce a given volume of vapor also increases. The required latent heat of vaporization for bubble formation is provided by the surrounding liquid, which is cooled as a result, and a thermal boundary layer forms around the cavitation bubble. With increasing fluid temperature, the energy required to produce a given volume of vapor increases, which also increases this thermal boundary layer effect. At some point, this relatively cool thermal boundary that forms around the cavitation bubble will act as an insulator against more energy transfer from the surrounding liquid and will limit further bubble growth. This is the explanation why a pump has a lower NPSHr when pumping a hotter medium.

Figure 30 and Figure 31 show NPSH test results for water at different temperatures. As seen in the figures, NPSHr for the pump decreases with increasing water temperature. Although the thermal suppression effect is observed at all the temperatures, its impact on NPSHr becomes significant only as the water temperature approaches 200 ºF.

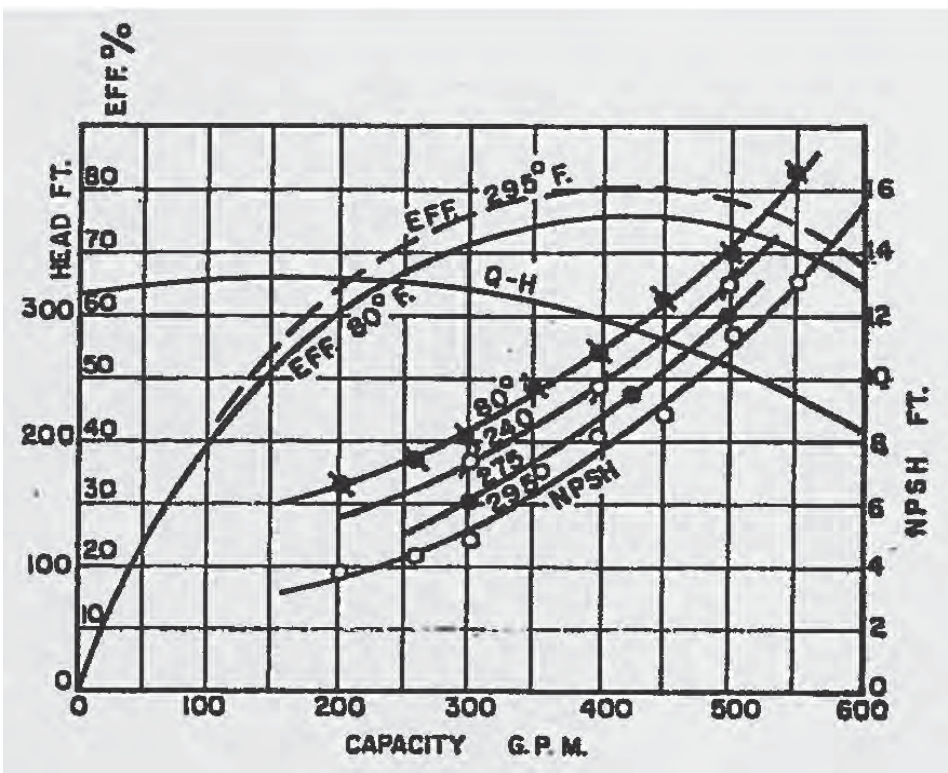

Figure 30: NPSHr Curves for Varying Temperatures (Stepanoff, 1965) [2]

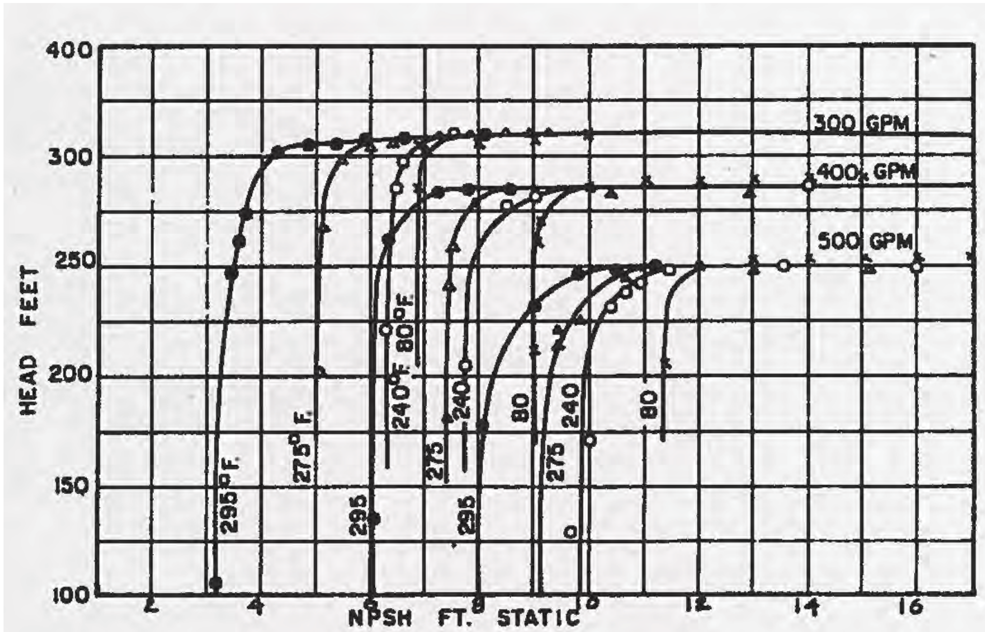

Figure 31: NPSH Knees at Different Temperatures (Stepanoff, 1965) [2]

To provide a method to account for this thermal suppression phenomenon, Gulich [1] and Stepanoff [2] developed similar equations for predicting the change in NPSHr resulting from a change in pumpage temperature. Figure 32, which is based on Gulich's TSH equations for water, can be used for predicting the influence of temperature on various cavitation parameters including NPSH3. ANSI/HI standard 1.3, Rotordynamic (Centrifugal) Pump Applications [14], contains an NPSHr correction chart for water temperature (reproduced as Figure 33) which predicts similar NPSHr reduction as Gulich's chart for the given temperature range.

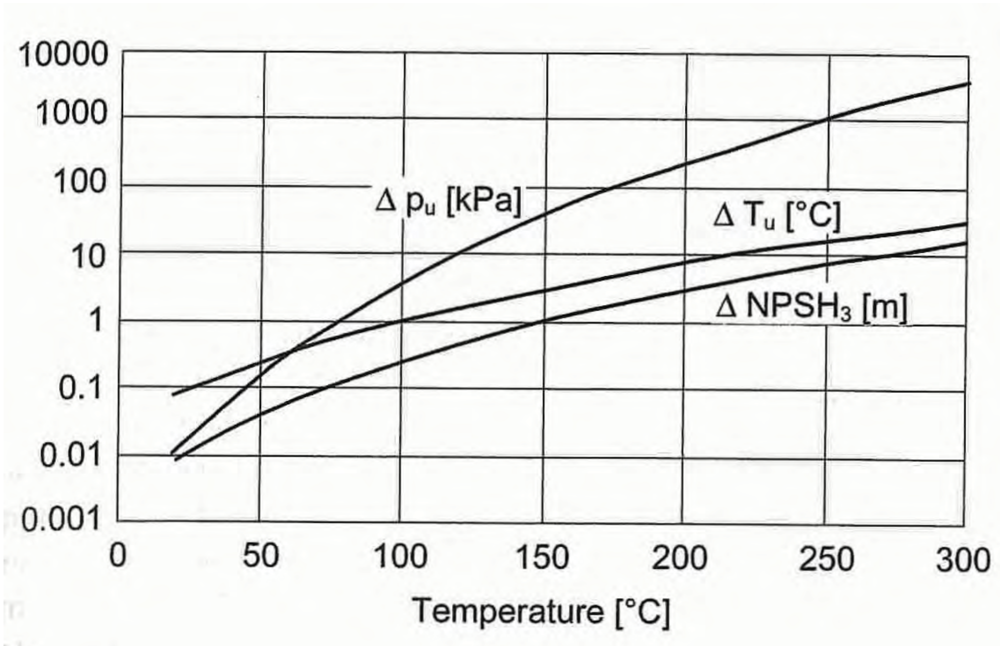

Figure 32: Cavitation Parameter Prediction Curve (Gulich) [1]

During a DBA-LOCA, the Monticello RHR pumps are postulated to operate in the temperature range of [[ ]]. For this temperature range, Figure 32 predicts a reduction in NPSH3 of approximately [[ ]] and [[ ]]. Therefore, with a test NPSHr of [[ ]], the maximum expected reduction in NPSHr for the CVDS pumps is [[ ]].

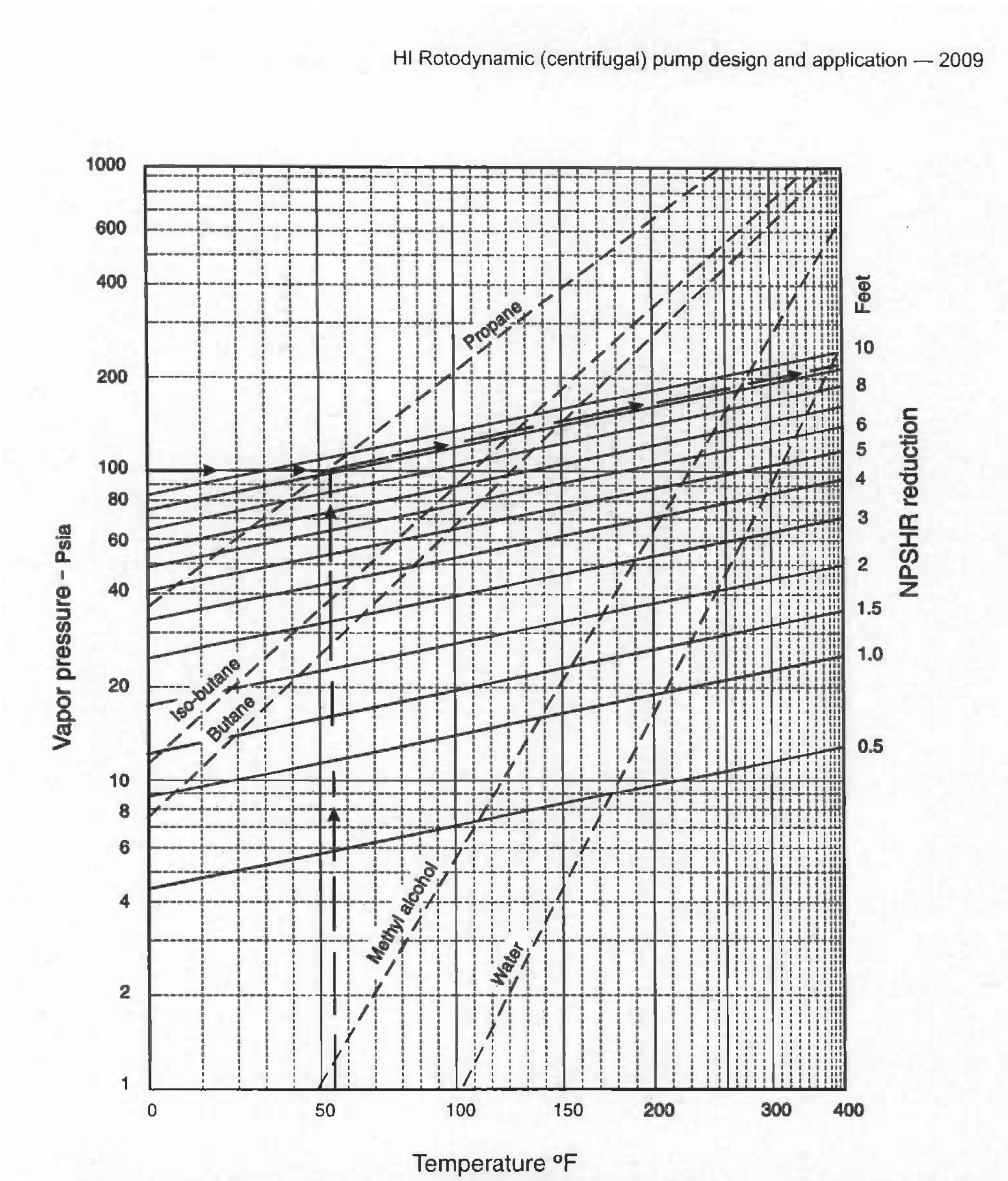

Figure 33: ANSI/HI 1.3 - NPSHr Temperature Correction Chart

2.3 Effect of Dissolved Air on NPSHr

The solubility of air in water depends on air pressure and water temperature. Solubility is a weak function of pressure (increases with increasing pressure) and decreases strongly with increasing water temperature [13]. Since BWR containments are maintained near atmospheric pressure, the amount of dissolved gas in the suppression pool water would be based on the gas saturation solubility at atmospheric pressure and the pool water temperature.

Research shows that small amounts of dissolved gases (approximately 0.5-2% by volume fraction) do not cause any significant impact on a pump's discharge performance. It has also been demonstrated that the introduction of small amounts of air can actually reduce pump noise, vibration, and cavitation damage by absorbing some of the implosion energy of the cavitating bubbles. Budris and Mayleben [6] investigated the impact of entrained gases on suction pulsation pressures and NPSHr. In their study, end suction pumps were injected with measured amounts of air at the suction inlet. It was observed that as the Gas Void Fraction (GVF) was increased from 0 to 0.5%, a significant reduction in suction pulsation pressure became evident. In another experiment for this study, NPSHr tests were conducted on pumps with and without air injection. It was found that injection of 0.5-2% of air GVF increased the NPSHr by about 7%.

The increase in NPSHr with an increase in the entrained gas GVF can be explained by the hypothesis that gas blockage is created at the impeller eye. This blockage leads to an increase in flow velocities at the impeller eye further reducing the static pressure and reducing the flow incidence on the impeller blades, which has the effect of shifting cavitation bubbles towards the blade pressure surface. Therefore, if a sufficient quantity of dissolved gas came out of solution due to the local pressure drop in a pump suction, conceivably a partial blockage could result. It is, however, unlikely that all of the dissolved gas would immediately come out of solution. The bulk of gas bubbles that do evolve would simply pass through the pump into the discharge stream.

2.3.1 Literature Search Results

A French study [10] conducted by Technical Centre for Mechanical Industries investigated the effects of entrained air and dissolved air on the NPSHr of pumps. Two pumps were used for this study. Pump A operated with an open loop system and had air injected into the pumpage. Pump B was run in a closed loop system and the system was slowly depressurized to reduce the percentage of dissolved oxygen in the pumpage (since solubility decreases with decrease in pressure). NPSHr (3% head breakdown) tests were conducted at three different flow rates for each pump. Precise measurements of entrained air and dissolved oxygen were recorded at regular intervals at each flow rate. It was found that Pump A (open loop) did not experience a degradation in the suction performance at the high flow rate (5500 gpm) until after 3.5-4% air by volume was injected into the system. At the low flow rate (3600 gpm), 2-2.5% air by volume in the system resulted in a degradation in the suction performance. For Pump B the dissolved oxygen percentage was lowered by depressurization, but no change was observed in the suction performance. The report concluded that the dissolved oxygen has no significant influence on the NPSHr of a pump. Moreover, the effect of entrained air on NSPHr is significant only after the pumpage has a GVF of at least 2-4% or more.

2.3.2 Approach for Estimating Impact of Dissolved Gas on NPSHr

Based on the gas blockage hypothesis stated earlier, Sulzer conducted a theoretical analysis to predict the degradation of pump discharge head and NPSHr resulting from the presence of dissolved gas in Monticello's RHR pumps. The following conservative assumptions were made for the analysis.

a) [[

]]

[[

]]

[[

]]

Figure 34: Monticello RHR Pump - Effect of Dissolved Gas (2% GVF) on NPSHr

[[

]]

[[

]]

2.4 Effect of Wear Ring Clearance on NPSHr

Wear rings provide a throttling clearance between the rotor and the stator of a pump. During pump operation, a small percentage of the impeller outlet flow leaks through the wear rings back into the impeller inlet as shown in Figure 35. The amount of leakage depends on the wear ring clearance and the pressure difference between the impeller inlet and exit. Increasing wear ring clearance increases the leakage flow and the flow through the impeller and, therefore, reduces the generated head at a given discharge flow rate. Increased impeller flow also leads to decreased pump efficiency and an increased NPSHr.

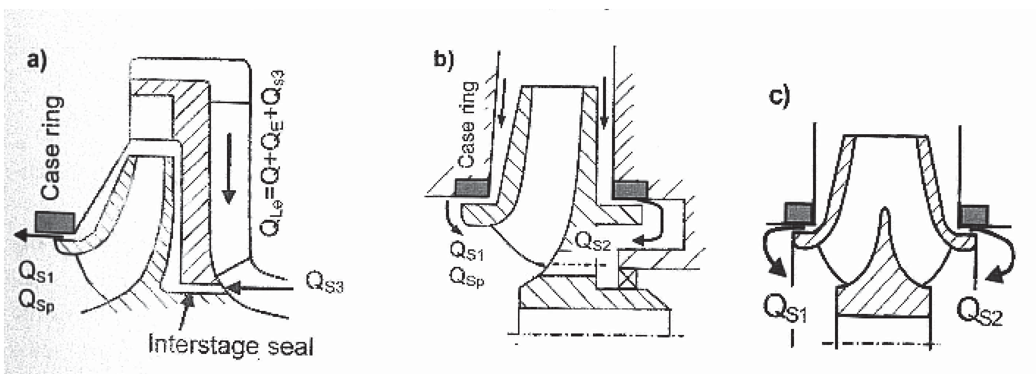

Figure 35: Wear Ring Leakage (Gulich)

2.4.1 Browns Ferry CFD Study on Wear Ring Clearances

A CFD study was conducted by Sulzer [5] using ANSYS CFX software to determine the effect of wear ring clearance on a Browns Ferry single stage RHR CVIC pump. 3-D models for the CFD analysis were set-up with nominal clearances (as designed (new) condition) and at two times the nominal clearances (worn out clearances). CFD was used for both set-ups at normalized flow rates of 0.75, 1.0, and 1.3 times the BEP flow rate [[ ]]. NPSH3 results from the CFD analysis are provided in Figure 36. [[

]]

[[

]]

Figure 36: Impact of Wear Ring Clearance on NPSHr of Browns Ferry RHR Pump Using CFD

2.4.2 Approach for Estimating Impact of Wear Ring Clearance on NPSHr

The contribution to the NPSHr uncertainty due to an increase in wear ring clearance depends on the wear ring clearance at the beginning of the DBA-LOCA event and any additional wear accrued during the mission time. Based on a BWROG survey of member plants, operating hours for RHR pumps is typically much less than [[ ]]. This amount of ordinary use is small compared with the expected life of a pump wear ring, which, depending on pumpage and wear ring material, may be equivalent to several years of continuous pump operation. The infrequent pump operation combined with actual plant-specific operating experience (pump maintenance frequency) and periodic pump surveillance testing, which monitors and trends pump performance, collectively provide reasonable assurance that the pump wear ring clearance prior to the LOCA will be within required tolerances. The additional pump duty accrued during a [[ ]] time for analyzed events is [[ ]], which again is small compared to the expected life of impeller wear rings. Should examination of plant data conclude that wear ring wear is small, then the wear ring contribution to the overall NPSH uncertainty would also be small and, thus, may be omitted from the NPSH uncertainty assessment.

However, where examination of plant data indicates that the wear ring wear is not small enough to be neglected, it is prudent to determine what the resulting effect could be on NPSH uncertainty. Therefore, Sulzer performed a 1-dimensional (1-D) theoretical analysis similar to the dissolved gas analysis discussed earlier to estimate the change in NPSHr due to an increase in the wear ring clearance for Monticello RHR pumps. [[

]]

[[

]]

Since a normal operating CVDS pump (configured and operating within the manufacturer's specifications and guidelines) is not expected to experience any appreciable increase in wear ring clearance during [[ ]] of operation, a conservative estimate of the maximum effect of increased wear ring clearance on NPSHr uncertainty can be estimated using the analysis approach above. [[

]]

[[

]]

Figure 37: Monticello RHR Pump - Effect of [[ ]] **Wear Ring Clearance on NPSHr**

[[

]]

[[

]]

Figure 38: Browns Ferry - CFD v/s 1-D Theoretical Method

As noted, the magnitude of NPSHr uncertainty contribution from the wear rings is primarily a function of the wear ring clearance prior to the DBA-LOCA event. Since a pump could be near the end of expected life, have some wear, or have been recently overhauled (new condition), a statistical treatment may be used to assess the NPSHr uncertainty contribution of this variable. The statistical approach is presented in Section 3.0.

3.0 Combined NPSHr Uncertainties

The primary intent of this report is to establish a methodology to quantify both the individual and combined uncertainty contributions of various system and pump related variables on NPSHr. The effects of the following pump related variables were examined: 1) plant piping geometry 2) fluid temperature 3) dissolved gas and 4) wear ring clearance.

[[

]]

[[

]]

Regarding wear ring effects, where examination of plant data concludes that pump wear ring wear is small, then the wear ring contribution to the overall NPSHr uncertainty will also be small and it may be excluded from the NPSHr uncertainty assessment. However, should examination of plant data conclude that pump wear ring wear is not small enough to be excluded from the overall NPSHr uncertainty assessment, then the wear ring contribution should be included in the overall NPSHr uncertainty as outlined below.

[[

]]

[[

]]

[[

]]

[[

]]

4.0 Conclusions

This report outlined analytical methods for determining the impact of various pump parameters on the overall NPSHr uncertainty of the pump. Each of the methodologies presented were derived using a blend of theoretical analysis, research papers, test results, and the CFD data obtained for similar type pumps. The NPSHr uncertainty computed using the analytical methods provides a conservative estimate of the combined effects from several different, independent variables that can affect the pump NPSHr. The effects of pump suction piping geometry, pump speed, pump test instrumentation uncertainty, pumped liquid temperature, pumped liquid dissolved gas, and pump wear ring clearances have all been, to the extent reasonably practical, quantified and combined to express a total NPSHr uncertainty for a Sulzer CVDS pump used in the RHR system at Monticello Nuclear Generating Plant.

Although the analytical methods discussed in this report can be applied to other pump/plant applications it is important that a thorough analysis of the pump design and system specifics be conducted to determine an appropriate NPSHr uncertainty value for each parameter. For example, if the temperature of the suppression pool feeding the pump is high [[ ]], then the probability of dissolved gases being present in the system is low. If a plant/pump has a suction piping design which causes fewer distortions in the inlet flow, then a value lower than the [[ ]] NPSHr uncertainty, as given in this report can be applied. [[

]] It is important that an engineering justification is provided if the user intends to use values lower than the NPSHr uncertainty values provided in this report.

This report presented a statistical method for combining NPSHr uncertainty values for obtaining an overall NPSHr uncertainty for the Monticello CVDS RHR pump. This method utilizes the general approach adopted for combining random and systematic uncertainties and it has been used with the intention of providing a conservative overall NPSHr uncertainty for the pump. However, the statistical method provided in this report is neither a pump industry standard nor has it been validated through pump testing or CFD analysis. Therefore, it is recommended that this approach be used judiciously by the pump/plant users for application to other pump types and operating conditions.

The results in this report serve to provide reasonable assurance that an NPSHr uncertainty less than [[ ]] should be expected for the pump in this specific service application. Noteworthy among these uncertainty contributors is allowance for a pump speed variation of up to [[ ]] which provides sufficient margin to accommodate variations of EDG over-frequency within Technical Specification limits and motor slip. Also included are wear ring clearance effects. When considering the effects of both dissolved gas (inlet GVF) and increased wear ring clearance, the interaction of the resultant degraded pump curve and the system curve must be considered. The effective change in NPSHr due to these two factors will be much lower than their apparent impact if a constant flow rate is assumed.

Generic applicability and limitations:

Generic applicability, cautions and limitations on the use of specific values provided within this and related contributing tasks include the following:

- Speed uncertainty methodology [11] can be generically applied to directly coupled motor driven pumps
- Test instrumentation uncertainty methodology [12] can be generically applied to most any pump while the specific uncertainty value cited in the report are applicable to the Sulzer pumps with similar operating parameters (head, flow, and RPM) as the Monticello RHR pumps
- The magnitude of the temperature effects can be generically applied to any BWR ECCS pumps taking suction from the suppression pool with peak pool temperatures in the range of [[ ]]
- Dissolved gas uncertainty should be limited to pumps of similar hydraulic design as the Sulzer CVDS pumps used for RHR service at Monticello NPS operating at a similar relative point on their pump curves and taking suction from a suppression pool with peak pool temperatures in the range of [[ ]]
- NPSHr uncertainty recommendations due to suction piping geometry are applicable to pumps with:
    - [[

]]

- Wear ring uncertainty effects should be evaluated on a plant specific basis. A methodology was developed for determining the magnitude of the NPSHr uncertainty contribution due to increased wear ring clearance. A procedure, based on plant specific maximum wear ring clearance criteria and pump performance monitoring data, was developed to calculate the wear ring NPSHr uncertainty contribution. Finally, a representative example calculation, using the Monticello RHR pumps maximum wear ring clearance criteria, was presented to illustrate the uncertainty contribution due to wear ring clearance effects.

The results reported are representative for the specific evaluated application, the Monticello CVDS RHR pumps, and provide assurance that use of a generic [[ ]] NPSHr uncertainty for similar pumps in similar service conditions is a reasonable and bounding value.

5.0 Bibliography

1. Centrifugal Pumps, Johann Gulich, 2nd Edition, Chapter 6.
2. Pumps and Blowers Two-Phase Flow, Stepanoff.
3. Miriam Roth Kliem, Experimentelle und Numerische Untersuchung zum Einfluss von Einbaubedingungen auf das Betriebs – und Kavitationsverhalten von Kreiselpumpen, 2006.
4. Bujnes, J. H, Op De Woerd, J.,1984, "Erosion Free Operation of Cavitating Pump," Proceedings of the 2nd European Congress on Fluid Machinery for the Oil, Petrochemical and Related Industries, The Hague, The Netherlands, IMechE Conference Publications 1984-2, Paper C28.
5. CFD Study of Browns Ferry CVIC Pump, by Sulzer Innotec.
6. Allan R. Budris, Philip A. Mayleben, "Effects of Entrained Air, NPSH Margin, And Suction Piping on Cavitation in Centrifugal Pumps",1998.
7. Terry Henshaw, P. E, "Effect of Internal Clearances on NPSHR", Pumps and Systems, July 2009.
8. ANSI/HI 9.6.6-2009, America National Standard for Rotodynamic Pumps for Pump Piping, New Jersey.
9. Bruno Schiavello, " Visual Study of Cavitation – An Engineering Tool to Improve Pump Reliability," Proceedings of EPRI 1st international Conference on Improve Coal-Fired Power Plants, Palo Alto, California.
10. B. Le Fur (Mrs.), J. F. David, D.Le'cot "Influence de l'air occlus et dissous dans l'eau sur le comportement des pompes en cavitation", CETIM, Nantes
11. Ankur Kalra, "Task 2 – Equation for Pump Speed Correction Sulzer Pumps (US) Inc. Monticello – RHR & CS Pumps", Sulzer Report E12.5.1920, Nov 7, 2011.
12. Ankur Kalra, "Task 6 – NPSHr Test Instrumentation Accuracy Affect on the Published Results, Sulzer Pumps (US) Inc. Monticello – 12x14x14.5 CVDS RHR Pump", Sulzer Report E12.5.1914, Nov. 7, 2011.
13. Centrifugal Pumps, Johann Gulich, 2nd Edition, Appendix A, Figure A3.2.
14. ANSI/HI 1.3-2009, Rotodynamic (Centrifugal) Pump Applications